Dynamic Equivalent Representation for Symmetrical Short-Circuit Analysis of Power Systems with Power Electronics

Jie Song*, Josep Arévalo-Soler, Marc Cheah-Mane, Eduardo Prieto-Araujo and Oriol Gomis-Bellmunt
Departament d'Enginyeria Elèctrica, CITCEA, Universitat Politècnica de Catalunya
*Corresponding: jie.song@upc.edu

***Abstract*—Thévenin equivalent has been considered the standard power system representation for short-circuit analysis. However, the increasing penetration of power electronics in modern power systems introduces diversified short-circuit current responses which are not considered by conventional Thévenin equivalent. As an alternative, this paper proposes a different dynamic grid equivalent representation for short-circuit analysis of power systems with power electronics. The equivalent parameters are identified to accurately capture the dynamic short-circuit current responses contributed by power converters. Also, the equivalent parameters are varied from different depths of short-circuit fault in order to cover various fault conditions. The proposed grid equivalent has been tested and validated on studied systems with Voltage Source Converters (VSCs).**

***Index Terms*—Voltage Source Converter, short-circuit analysis, grid equivalent.**

I. Introduction

Short-circuit analysis is a fundamental task for operation, control and proper protection tuning of power systems [1], [2]. Thévenin and Norton equivalents have been widely adopted to represent the studied system for short-circuit analysis for decades. This is because these equivalents naturally emulate the fault dynamics of synchronous generators, which are considered as main sources of short-circuit current in conventional power systems [3]–[5]. Modern power systems are increasingly penetrated with power electronics converters while phasing out conventional synchronous generators. Power electronics converters are fully controllable devices with low inertial and very limited overload capability, which have a significantly different fault response compared to synchronous generators [6]. Therefore, the conventional Thévenin equivalent is not suitable for short-circuit analysis of power systems dominated by power electronics [7].

Comprehensive studies on dynamic fault responses of power converters have been reported in the literature. Dynamic transient fault current model of inverters-based distributed generators has been presented in [8], [9] considering converters' current limitation. The PLL dynamics and PI controller saturation effects have been included in [6], [10], [11] for short-circuit analysis of power-electronics-dominated systems. A dynamic fault model has also been developed for grid-forming converters in [12], [13]. These studies are implemented with the complete model of the studied system without involving the concept of equivalent. An accurate equivalent representation is still needed as it stands for an efficient tool for short-circuit analysis of power-electronics-dominated systems. This is especially critical for large-scale systems with many converters.

Several attempts have been reported in the references to obtain the grid equivalent representation for power systems with power converters. Simplified impedance model for power systems dominated by VSCs has been developed by reducing model order of AC grids [14] or converter control [15]. The equivalent impedance model of power-electronics-dominated systems has been also developed using data-driven techniques in [16], [17]. The studies focused on modeling in frequency domain and therefore are not suitable for simulations under large-signal disturbances (e.g. short-circuit fault).

On the other hand, equivalent model for dynamic transient analysis has been also investigated in the literature. Dynamic equivalent representation is obtained by aggregating several power converters with homogeneous control [18]–[21]. Equivalent model of power systems with power converters is also developed with system identification techniques [22], [23] and artificial neural networks [24]–[26]. However, the grid-support functions and current-saturated operation of power converters are not considered in these studies. Therefore, they are limited to normal operation and cannot be applied directly to short-circuit analysis.

Recent research interests have been raised for equivalent representation for short-circuit analysis but limited with steady-state approaches. In [27], fault current contribution from a type IV wind turbine is expressed with a voltage-dependent current source in order to accurately represent the operation of converters under different depths of fault. The similar equivalent representation has been also adopted for short-circuit calculation of wind power plants with type III turbines [28]. The authors of this paper have also proposed a different grid equivalent representation based on voltage-current mapping that can accurately capture the non-linear characteristics of power converters in steady-state (including short-circuit calculation) [29]. However, the steady-state approaches presented in [27]–[29] cannot be adopted directly for dynamic short-circuit analysis as they only aim to identify the steady-state equilibrium point and do not consider the fault dynamics.

This paper proposes a new equivalent representation for

short-circuit analysis of power systems with power electronics. The proposed equivalent aims to extend the usage of conventional Thévenin equivalent for not only steady-state conditions, but to fault dynamics. The equivalent is parameterized through short-circuit current measurements obtained from the studied system with various fault impedances. The studied system is expressed in single-phase with per-unit value assuming a balanced voltage condition. Symmetrical three-phase to ground faults have been studied for short-circuit analysis in this paper. The proposed dynamic equivalent representation has been tested in several VSCs-based studied systems and validated through comparison with simulation results from the complete model.

II. Overview of VSC Modeling for Short-Circuit Analysis

This paper first provides an overview of the VSC fault modeling, which is an essential component of modern power systems. The VSC can be modeled as a voltage source, $\underline{u}_v sc$, in series connection with a phase reactor, $\underline{z}_{vsc}$, following the equivalent scheme shown in Fig. 1.

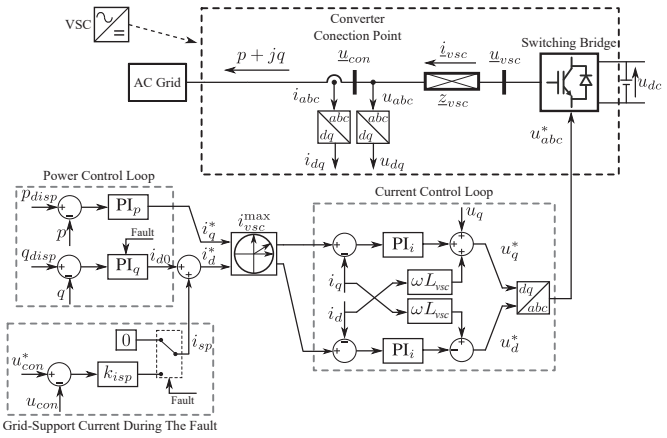

Fig. 1. VSC Equivalent Diagram and Control Scheme [30]

The VSC regulates the current exchange with the AC grid at the Converter Connection Point (CCP) following the control implementation. In particular, the current control loop tracks the current reference value in qd frame with a second-order response when ignoring the PLL dynamics [31]. However, more complicated characteristics will be added to the dynamic transient response of the VSC during the fault from the outer loop control.

In case of fault conditions, the converter still follows the constant active power reference, p_{disp}, while the reactive power injection will be modified to provide the voltage-support function required by the grid codes [32]. Therefore, the PI controller for reactive power will be frozen and hold the output current reference, i_{d0}. Also, a voltage-droop grid support will be activated and added to the reactive current reference i^*_d such that [30], [33]:

$$i^*_d = i_{d0} + k_{isp}(u^*_{con} - u_{con}) \tag{1}$$

where k_{isp} is the voltage-droop gain for the grid support current, u^*_{con} and u_{con} are respectively the reference and the measured value of the CCP voltage. The grid support function imposes coupling between the grid voltage dynamics and VSC current injection during the fault, which should be taken into consideration in short-circuit analysis.

In addition, the current-saturation block is included in the converter control to protect the semiconductor device from being over-loaded during the fault. This current-saturation block modifies the current reference value imposed on th current control loop to ensure the actual current injection magnitude from the converter will not exceed the maximum value during the fault. Typically, the active current element, i_q, is reduced in order to prioritize the reactive current, i_d. Therefore, depending on the current elements being saturated, three states (unsaturated-USS, partially saturated-PSS and fully saturated-FSS) are considered for the current-saturated operation of the converter [30], [33]:

$$\begin{cases} i^*_{q-sat} = i^*_q;\ i^*_{d-sat} = i^*_d & \text{USS} \\ i^*_{q-sat} = \sqrt{i^{\max 2}_{vsc} - i^{*2}_d};\ i^*_{d-sat} = i^*_d & \text{PSS} \\ i^*_{q-sat} = 0;\ i^*_{d-sat} = i^{\max}_{vsc} & \text{FSS} \end{cases} \tag{2}$$

where i^*_{q-sat} and i^*_{d-sat} are current references value imposes on the current control loop during the fault, $i^{\max}_{vsc}$ is the converter nominal current. The current saturation scheme modifies not only the converter set point in steady state but also the dynamic responses as it blocks the signal from the outer loop controller when the current limit has been reached.

It should be noticed that the grid-support control and the possible current-saturated operation lead to diversified responses of the converter with various fault conditions and different parameters of the employed controller [6]. These characteristics increase the complexity to obtain an effective grid equivalent representation for short-circuit analysis. This is especially for analysis of a studied system with several converters as they might have with various controller tuning and operate at different current saturation states during the fault.

III. Dynamic equivalent for short-Circuit Analysis

In this Section, a different dynamic equivalent has been proposed to accurately represent the studied system with power electronics for short-circuit analysis. In particular, the proposed equivalent is parameterized from dynamic simulations with various short-circuit fault impedances in order to capture the complex characteristics of the studied system.

A. Equivalent Parameter Estimation

In conventional power systems, the Thévenin equivalent parameters are typically calculated from steady-state equilibrium points (e.g. open-circuit and short-circuit operation points) [5]. However, such a static approach might fail to accurately capture the complex dynamic responses that arose from fault responses of power converters. References on the

short-circuit modeling of power converters suggest that the short-circuit current contribution from converters typically follows a second-order response, which can be represented with the Thévenin equivalent [8], [9]. However, the Thévenin equivalent parameters may vary from different fault conditions.

In this paper, the proposed equivalent representation adopts the same scheme as the conventional Thévenin equivalent. However, a different approach is adopted to identify Thévenin equivalent parameters in order to accurately represent the fault current response from a studied system with power electronics. With the Thévenin equivalent representation from the fault location, the short-circuit current response in s-domain, $i_{sc}(s)$, from the studied system with a tested short-circuit impedance, $\underline{z}_{sc}$, can be expressed as follows [34]:

$$i_{sc}(s) = \frac{k\omega_n^2}{s^2 + 2\xi\omega_n s + \omega_n^2} \tag{3}$$

where k is the DC gain, ξ is the damping factor and ω_n is the natural frequency. In particular, ξ and ω_n can be identified using curve-fitting techniques from the time-domain results of short-circuit current. In this paper, the transfer function estimation block implemented in MATLAB, *tfest*, is adopted to estimate the value of ξ and ω_n. In particular, the Levenberg-Marquardt least squares method with zero initial conditions has been adopted for curve-fitting for all case studies reported in this paper. The nature frequency ω_n can be considered as a constant, which is equal to the nominal frequency of the studied system, assuming the grid frequency variation during the fault can be neglected. While k is equal to the steady-state value of the short-circuit current, which can be identified from dynamic simulation. It should be also noticed that in real applications, the studied system does not always achieve the short-circuit equilibrium point depending on the dynamic responses and fault clearance time. However, in order to identify short-circuit current value, k, the fault duration should be long enough in the dynamic simulation. An alternative is to identify the short-circuit equilibrium point using a steady-state approach [30], [33].

The Thévenin equivalent voltage, u_{th}^{eq}, can be identified from the pre-fault voltage at the fault location. Then, the Thévenin equivalent impedance, $\underline{z}_{th}^{eq}$, can be calculated by solving the following equations:

$$\begin{cases} k = |u_{th}^{eq}/(\underline{z}_{th}^{eq} + \underline{z}_{sc})| \\ \xi = \Re(\underline{z}_{th}^{eq} + \underline{z}_{sc})/\Im(\underline{z}_{th}^{eq} + \underline{z}_{sc}) \end{cases} \tag{4}$$

Such curve-fitting practice based on dynamic simulation results could ensure that the obtained equivalent could accurately represent the fault current response of the studied system with a specific fault condition. It should be noticed that various curve fitting techniques can be adopted in different applications. Additional studies can be performed to compare the accuracy and computing efficiency of different methods.

B. Mapping of Equivalent Impedance

It can be observed that the Thévenin equivalent voltage is determined by the pre-fault equilibrium point of the studied system and therefore is unvaried with different short-circuit fault impedances. However, the Thévenin equivalent impedance is identified considering both the steady-state value and dynamic response of the short-circuit fault current. Therefore, the Thévenin equivalent impedance might vary from different tested short-circuit impedance values.

This paper proposes to map the Thévenin equivalent impedance for various short-circuit impedances in order to build the dynamic equivalent representation that covers different fault conditions. Similar sampling-points based techniques have been adopted by the authors of this paper to develop the steady-state grid equivalent in [29] and to analyze the steady-state grid strength in [35].

The proposed methodology to obtain the Thévenin equivalent impedance map is summarized as shown in Algorithm 1. The required input information of the algorithm includes the Thévenin equivalent voltage, u_{th}^{eq}, vectors of tested short-circuit impedance magnitudes, Z_{sc}, and angles, Θ_{sc}. In particular, the Thévenin equivalent voltage can be identified from the pre-fault operation point through power flow calculation or dynamic simulation.

The short-circuit impedance, $\underline{z}_{sc}$, is tested with N_m different magnitudes and N_a angles. Sampling points are properly selected in order to cover the certain operation range of the studied system in terms of fault impedance magnitudes and angles. The constructed equivalent is only valid for short-circuit analysis with the fault impedance within such range.

Dynamic simulations will be executed with each tested short-circuit impedance, $\underline{z}_{sc} = Z_{sc}(n_m)\angle\Theta_z(n_a)$, inserted to the fault location as the disturbance to the studied system. The damping factor, ξ, can be identified through curve fitting from the time-domain results of the short-circuit current, $i_{sc}(t)$. The corresponding Thévenin equivalent impedance, $\underline{z}_{th}^{eq}$, can be calculated following (4). Then, an interpolated function, F_{eq}, can be obtained from data interpolation of the obtained Thévenin equivalent impedance map corresponding to various short-circuit impedance magnitudes and angles. In this paper, such interpolant function is obtained using the *scatteredInterpolant* function from MATLAB. As the result, the Thévenin equivalent impedance of the studied system corresponding to any tested short-circuit fault impedance can be estimated from the identified interpolant function such that:

$$\underline{z}_{th}^{eq} = F_{eq}(z_{sc}, \theta_z) \tag{5}$$

An alternative of the mapping to short-circuit impedance is to match the equivalent parameters to various fault voltage values, $\underline{u}_{sc}$. The fault voltage can be obtained by performing the steady-state short-circuit calculation [36]. However, it is more straightforward to adopt the mapping to short-circuit impedance expressed in (5) as typically the fault scenario is defined by the fault impedance value instead of the fault voltage.

It should be also noticed that with a larger number of sampling points, $N_m \times N_a$, the accuracy of the obtained grid equivalent can be improved. However, higher computing time will be required to execute simulations to build the equivalent.

Algorithm 1: Obtaining Thévenin equivalent impedance map

input : Thévenin equivalent voltage, u_{th}^{eq}, tested short-circuit impedance magnitudes, Z_{sc}, and angles,Θ_z
output: Interpolated function F_{eq}

begin
  for $n_m \leftarrow 1$ **to** N_m **do**
    for $n_a \leftarrow 1$ **to** N_a **do**
      $\underline{z}_{sc} = Z_{sc}(n_m)\angle\Theta_z(n_a)$;
      excute simulation with $\underline{z}_{sc}$, $\xi = tfest(i_{sc}(t))$;
      calculate $\underline{z}_{th}^{eq}$ following (4);
      $Z_{eq}(n_m, n_a) = \underline{z}_{th}^{eq}$;
    end
  end
  $F_{eq} = Interpolate(Z_{sc}, \Theta_z, Z_{eq})$, **return** F_{eq}
end

IV. Case Studies

The proposed dynamic equivalent representation is implemented and validated with test systems with VSCs in this Section.

A. Test System 1

The first test system is formed by the AC grid Thévenin equivalent and a VSC in PQ control with the fast reactive current injection during the fault to support the grid voltage following the equivalent model expressed in [33]. With the dynamic equivalent proposed in this paper, the studied system can be expressed with the Thévenin equivalent from the fault location as shown in Fig. 2. The parameters of this test system are listed in Table I from the Appendix.

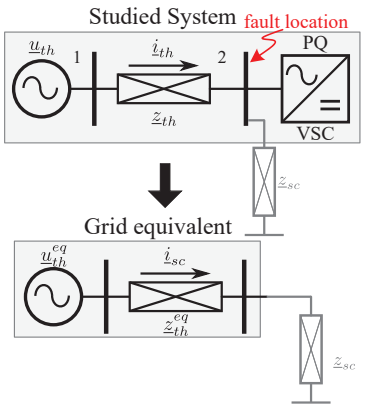

Fig. 2. Proposed grid equivalent for short-circuit analysis

In order to obtain the grid equivalent parameters, dynamic simulations have been performed with several short-circuit fault impedance values following Algorithm 1. In particular, the fault impedance has been tested with the magnitude varied from 0.01 to 1 pu and the angle from 60° to 90°. The identified Thévenin equivalent impedance map is shown in Fig. 3. In particular, the identified equivalent impedance is visualized in terms of the real part, r_{th}^{eq}, and the imaginary part, x_{eq}^{th}, corresponding to each tested fault impedance magnitude, z_{sc}, and angle, θ_z.

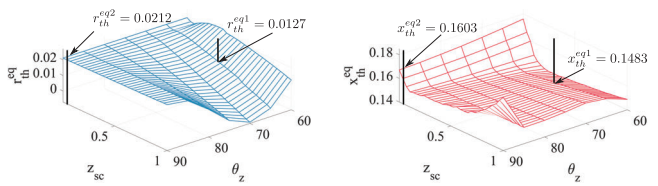

(a) Resistance (b) Reactance

Fig. 3. Identified Thévenin equivalent impedance map

Short-circuit analysis has been performed with two different fault impedances, $\underline{z}_{sc1} = 0.5\angle 65°$ and $\underline{z}_{sc2} = 0.05\angle 90°$, inserted at the fault location indicated as shown in Fig. 2. The tested fault impedance has been selected to represent a moderate and a severe fault condition. However, the constructed equivalent can be also adopted to simulate different fault scenarios. The Thévenin equivalent voltage, u_{th}^{eq}, is unvaried with different short-circuit impedance and can be identified from the pre-fault equilibrium point as explained previously in Section III-A. While the Thévenin equivalent impedance can be identified from the interpolant function expressed in (5). The identified Thévenin equivalent impedances, $\underline{z}_{th}^{eq1} = r_{th}^{eq1} + jx_{th}^{eq1}$ and $\underline{z}_{th}^{eq2} = r_{th}^{eq2} + jx_{th}^{eq2}$, can be also expressed as intersection points between each tested short-circuit impedance and the impedance map surface as marked in Fig. 3.

Dynamic simulations have been performed with both the grid equivalent representation and the complete model of the original studied system from MATLAB Simulink. In particular, the short-circuit impedance has been inserted to the fault location, which represents the disturbance to the studied grid. The time-domain simulation results of the short-circuit current magnitude, i_{sc}, are shown in Fig. 4 for the two different tested short-circuit impedances. It can be observed that the dynamic simulation results obtained from the grid equivalent representation proposed in this paper match with the results from the complete model.

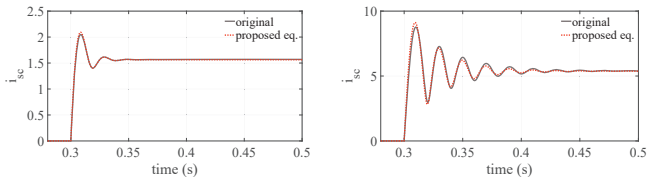

(a) $\underline{z}_{sc1} = 0.5\angle 65°$ pu (b) $\underline{z}_{sc2} = 0.05\angle 90°$ pu

Fig. 4. Comparison of short-circuit current magnitude in Test System 1

The grid equivalent has also been developed for Test Systems 1 with different sizes of the VSC. In particular, the VSC has been tested with several values for the nominal current, i_{vsc}^{max}. The active power reference, p_{ref}, and the droop gain for voltage-support control during the fault, k_{isp}, are modified in proportion to i_{vsc}^{max} for the VSC. For visualization purposes, the short-circuit impedance has been tested with a fixed angle $\theta_z = 90°$ and sweeping various magnitudes. The identified Thévenin equivalent impedances corresponding to different

sizes of the VSC in the studied system are shown in Fig. 5. It can be observed that without penetration of the VSC (i.e. $i_{vsc}^{max} = 0$), the identified grid equivalent impedance is constant with different depths of fault. In particular, the grid equivalent impedance is only determined by the AC grid impedance in the studied system such that: $\underline{z}_{th}^{eq} = \underline{z}_{th}$. However, with an increased size of the VSC, the identified grid equivalent impedance, $\underline{z}_{th}^{eq}$, deviates more from AC grid impedance, $\underline{z}_{th}$, as both the dynamics and steady-state equilibrium point during the short-circuit fault depends more on the VSC operation. This is especially critical for the inductive element, x_{th}^{eq}, and the resistive element, r_{th}^{eq}, with a low fault impedance.

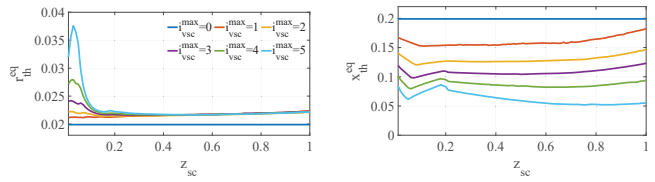

(a) Resistance (b) Reactance

Fig. 5. Identified Thévenin equivalent impedance with different size of VSC in Test System 1

B. Test System 2

The second test system of a PV power plant consists of 48 PV generation units (which are expressed with their AC side inverter model for short-circuit analysis) and the main AC grid expressed with the Thévenin equivalent with the scheme shown in Fig. 6. The test system parameters and PV inverters control are detailed in [33]. However, the proposed equivalent can be also applied to grids involving other types of inverter-based resource, such as wind power plants, as long as the complete dynamic simulation model is provided.

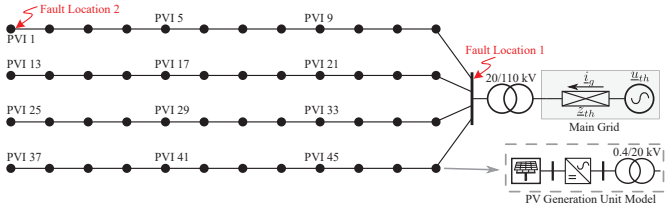

Fig. 6. Scheme of Test System 2

Short-circuit analysis is performed with two different fault locations as indicated in Fig. 6. Therefore, grid equivalents are constructed to represent the studied system respectively from the two fault locations. The same range of short-circuit impedances shown in Fig. 3 have been tested in order to identify the Thévenin equivalent impedance map of Test System 2.

The identified Thévenin equivalent impedance from Fault Location 1 is shown in Fig. 7. It can be observed that the identified Thévenin equivalent impedance is approximately equal to the main grid equivalent impdance in the studied system for most of tested fault cases. This is because the fault current responses are dominated by the main AC grid. However, when the short-circuit fault is tested with a high fault impedance and a fault impedance angle $\theta_z = 70°$, an increase RX ratio can be observed from the identified equivalent impedance.

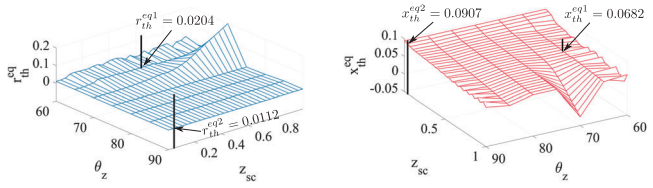

(a) Resistance (b) Reactance

Fig. 7. Thévenin equivalent impedance map of Test System2, Fault Location 1

Short-circuit analysis has been performed with the two different fault impedances, $\underline{z}_{sc1} = 0.5\angle 65°$ and $\underline{z}_{sc2} = 0.05\angle 90°$, which are respectively inserted at Fault Location 1 shown in Fig. 6. The Thévenin equivalent impedance values are marked in Fig. 7 for each tested short-circuit fault impedance. The time-domain results of the short-circuit current from both the constructed grid equivalent representation and the complete model of Test System 2 are shown in Fig. 8.

In addition, the simulation results have been obtained from conventional Thévenin equivalent, which are shown with green dashed curves in Fig. 8. In particular, the conventional Thévenin equivalent is parameterized with the steady-state equilibrium points in normal operation and during the fault with a low fault impedance. It can be observed that the conventional Thévenin equivalent generates more significant error compared to the equivalent proposed in this paper both in steady-state and during the fault transient. This is specially critical for the case with a low fault impedance as the obtained short-circuit fault waveform shows significantly higher damping time.

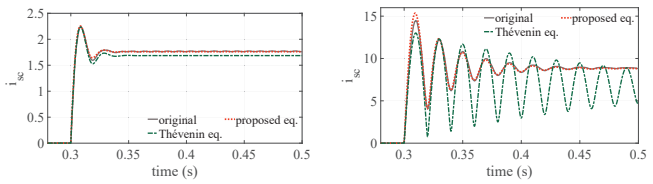

(a) $\underline{z}_{sc1} = 0.5\angle 65°$ pu (b) $\underline{z}_{sc2} = 0.05\angle 90°$ pu

Fig. 8. Comparison of short-circuit current magnitude in Test System 2, Fault Location 1

With a remote fault at Fault Location 2, the short-circuit current dynamics are dominated by the operation of PV inverters. Therefore, the identified Thévenin equivalent impedance map, which is shown in Fig. 9, varies significantly from the equivalent model obtained from Fault Location 1. In particular, the magnitude of the Thévenin equivalent is higher compared to Fault Location 1 as the short-circuit current magnitude is reduced with a remote fault. Also, the identified equivalent impedance varies from different tested short-circuit fault impedances due to the complex operational characteristics from the large number of PV inverters in the studied system.

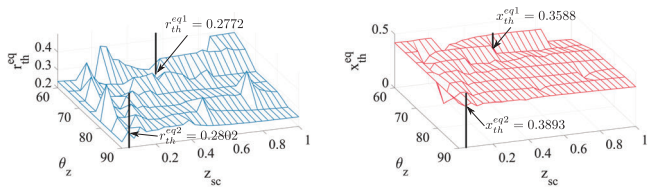

(a) Resistance (b) Reactance

Fig. 9. Thévenin equivalent impedance map of Test System2, Fault Location 2

Dynamic simulations results of short-circuit current are obtained from both the constructed grid equivalent representation and the complete model as shown in Fig. 10. It can be observed that the obtained equivalent representation delivers the accurate results compared to the original dynamic simulation model.

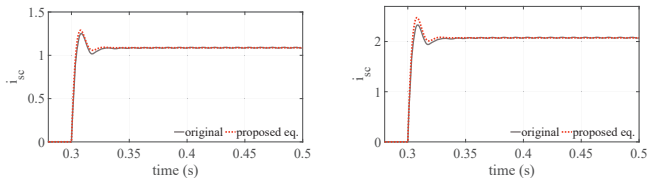

(a) $z_{sc1} = 0.5\angle 65^\circ$ pu (b) $z_{sc2} = 0.05\angle 90^\circ$ pu

Fig. 10. Comparison of short-circuit current magnitude in Test System 2, Fault Location 2

V. Conclusion

This paper proposes a dynamic equivalent representation for short-circuit analysis of power systems with power electronics. The constructed grid equivalent follows the same scheme as the Thévenin equivalent. In particular, the equivalent impedance values are identified from the time-domain results of the short-circuit current considering both the steady-state equilibrium point and dynamic responses. In addition, the equivalent impedance values are expressed as a map corresponding to various short-circuit fault impedances in order to obtain the grid equivalent representation for different fault conditions. This is different from the conventional Thévenin equivalent which has a static format.

The proposed grid equivalent has widely potential applications in analysis and protection design of power systems related to fault conditions with several benefits: compared to conventional Thévenin equivalent, the proposed grid equivalent can accurately represents the complex fault responses of a grid dominated by power electronics; compared to other analytical equivalents (reduced or aggregated converter modeling), the construction of the proposed equivalent can be automatized for studied systems with different configurations; compared to short-circuit analysis with the complete model, the grid equivalent representation can save the time to execute the dynamic simulation without compromising the accuracy; the proposed grid equivalent also stands for a new format of information that can be delivered from the system operators to power system designers when the complete model is not available due to the data privacy constraints.

Further studies can be performed to extend the grid equivalent proposed in this paper to cover the unbalanced voltage conditions with different types of faults. In particular, both the equivalent expression and the method to obtain the equivalent needs to be revised in order to accurately capture and characterize the studied system response with an asymmetrical fault. Also, more case studies can be carried out to the studied systems with power converters in different control modes (e.g. grid-forming).

Appendix

Table I includes the parameters of Test System1. Test System 2 parameters can be found in [33].

TABLE I
Parameters of Test System 1

Parameter	Value	Parameter	Value
Base value for per-unit system			
S_{base}	20 MVA	U_{base}	110 kV
Studied system parameters in pu			
u_{th}	1	z_{th}	$0.02 + j0.10$
$i_{vsc}^{\max}$	1	p_{disp}	0.5
q_{disp}	0	k_{isp}	2
u_{con}^{*}	1		

References

[1] M. M. Alam, H. Leite, J. Liang, and A. da Silva Carvalho, "Effects of vsc based hvdc system on distance protection of transmission lines," *International Journal of Electrical Power & Energy Systems*, vol. 92, pp. 245–260, 2017.

[2] L. Strezoski, M. Prica, and K. A. Loparo, "Generalized δ-circuit concept for integration of distributed generators in online short-circuit calculations," *IEEE Transactions on Power Systems*, vol. 32, no. 4, pp. 3237–3245, 2017.

[3] J. C. Das, *Power system analysis: short-circuit load flow and harmonics (2nd ed.)*. CRC Press, 2007.

[4] H. Saadat, *Power System Analysis*. McGraw-Hill, 2009.

[5] P. C. Krause *et al.*, *Analysis of Electric Machinery and Drive Systems*. Hoboken, NJ: Wiley, 2002.

[6] Q. Zhang *et al.*, "Fault modeling and analysis of grid-connected inverters with decoupled sequence control," *IEEE Transactions on Industrial Electronics*, vol. 69, no. 6, pp. 5782–5792, 2022.

[7] I. Kim, "Short-circuit analysis models for unbalanced inverter-based distributed generation sources and loads," *IEEE Transactions on Power Systems*, vol. 34, no. 5, pp. 3515–3526, 2019.

[8] Z. Shuai *et al.*, "Fault analysis of inverter-interfaced distributed generators with different control schemes," *IEEE Transactions on Power Delivery*, vol. 33, no. 3, pp. 1223–1235, 2018.

[9] T. Bi, B. Yang, K. Jia, L. Zheng, Q. Liu, and Q. Yang, "Review on renewable energy source fault characteristics analysis," *CSEE Journal of Power and Energy Systems*, vol. 8, no. 4, pp. 963–972, 2022.

[10] K. Jia *et al.*, "Transient fault current analysis of iiress considering controller saturation," *IEEE Transactions on Smart Grid*, vol. 13, no. 1, pp. 496–504, 2022.

[11] Q. Liu *et al.*, "Analytical model of inverter-interfaced renewable energy sources for power system protection," *IEEE Transactions on Power Delivery*, vol. 38, no. 2, pp. 1064–1073, 2023.

[12] C. Fang *et al.*, "Analysis of grid-forming iidg's transient- and steady-state fault model," *IEEE Transactions on Smart Grid*, vol. 13, no. 2, pp. 1187–1199, 2022.

[13] Q. Zhang *et al.*, "Fault modeling of grid-forming converters using dynamic phasor theory," in *2021 IEEE/IAS Industrial and Commercial Power System Asia*, pp. 1011–1016, 2021.

[14] G. Grdenić, M. Delimar, and J. Beerten, "Ac grid model order reduction based on interaction modes identification in converter-based power systems," *IEEE Transactions on Power Systems*, vol. 38, no. 3, pp. 2388–2397, 2023.
[15] G. Grdenić, F. J. C. García, N. d. M. D. Campos, F. Villella, and J. Beerten, "Model order reduction of voltage source converters based on the ac side admittance assessment: From emt to rms," *IEEE Transactions on Power Delivery*, vol. 38, no. 1, pp. 56–67, 2023.
[16] L. Fan *et al.*, "Data-driven dynamic modeling in power systems: A fresh look on inverter-based resource modeling," *IEEE Power and Energy Magazine*, vol. 20, no. 3, pp. 64–76, 2022.
[17] M. Zhang *et al.*, "Data-driven modeling of power-electronics-based power system considering the operating point variation," in *2021 IEEE Energy Conversion Congress and Exposition (ECCE)*, pp. 3513–3517, 2021.
[18] X. Zha *et al.*, "Dynamic Aggregation Modeling of Grid-Connected Inverters Using Hamilton's-Action-Based Coherent Equivalence," *IEEE Transactions on Industrial Electronics*, vol. 66, no. 8, pp. 6437–6448, 2019.
[19] P. o. Hart, "Coherency Identification and Aggregation in Grid-Forming, Droop-Controlled Inverter Networks," *IEEE Transactions on Industry Applications*, vol. PP, no. c, pp. 1–1, 2019.
[20] D.-E. Kim *et al.*, "Dynamic equivalent model of wind power plant using an aggregation technique," *IEEE Transactions on Energy Conversion*, vol. 30, no. 4, pp. 1639–1649, 2015.
[21] H. Kikusato *et al.*, "Aggregation of radial distribution system bus with volt-var control," *Energies*, vol. 14, no. 17, 2021.
[22] L. D. P. Ospina, V. U. Salazar, and D. P. Ospina, "Dynamic equivalents of nonlinear active distribution networks based on hammerstein-wiener models: An application for long-term power system phenomena," *IEEE Transactions on Power Systems*, vol. 37, no. 6, pp. 4286–4296, 2022.
[23] P. Sharma, V. Ajjarapu, and U. Vaidya, "Data-driven identification of nonlinear power system dynamics using output-only measurements," *IEEE Transactions on Power Systems*, vol. 37, no. 5, pp. 3458–3468, 2022.
[24] A. Azmy *et al.*, "Artificial neural network-based dynamic equivalents for distribution systems containing active sources," *IEE Proceedings - Generation, Transmission and Distribution*, vol. 151, pp. 681–688(7), November 2004.
[25] Y. Zhou and P. Zhang, "Neuro-reachability of networked microgrids," *IEEE Transactions on Power Systems*, vol. 37, no. 1, pp. 142–152, 2022.
[26] T. Xiao, Y. Chen, S. Huang, T. He, and H. Guan, "Feasibility study of neural ode and dae modules for power system dynamic component modeling," *IEEE Transactions on Power Systems*, vol. 38, no. 3, pp. 2666–2678, 2023.
[27] R. Furlaneto, I. Kocar, A. Grilo-Pavani, U. Karaagac, A. Haddadi, and E. Farantatos, "Short circuit network equivalents of systems with inverter-based resources," *Electric Power Systems Research*, vol. 199, p. 107314, 2021.
[28] I. Kocar, Y. Chang, R. M. Furlaneto, A. Grilo-Pavani, A. Haddadi, and E. Farantatos, "Nonlinear network equivalents of systems with inverter based resources to study unbalanced faults in steady state," in *2022 IEEE Power & Energy Society General Meeting (PESGM)*, pp. 1–5, 2022.
[29] J. Song *et al.*, "Grid equivalent representation of power systems with penetration of power electronics," *IEEE Transactions on Power Delivery*, pp. 1–15, 2023.
[30] J. Song, M. Cheah-Mane, E. Prieto-Araujo, and O. Gomis-Bellmunt, "A novel methodology for effective short-circuit calculation in offshore wind power plants considering converter limitations," *Electric Power Systems Research*, vol. 211, p. 108352, 2022.
[31] L. Zheng, K. Jia, T. Bi, Y. Fang, and Z. Yang, "Cosine similarity based line protection for large-scale wind farms," *IEEE Transactions on Industrial Electronics*, vol. 68, no. 7, pp. 5990–5999, 2021.
[32] T. Kauffmann, U. Karaagac, I. Kocar, S. Jensen, E. Farantatos, A. Haddadi, and J. Mahseredjian, "Short-circuit model for type-iv wind turbine generators with decoupled sequence control," *IEEE Transactions on Power Delivery*, vol. 34, no. 5, pp. 1998–2007, 2019.
[33] J. Song *et al.*, "Short-circuit analysis of grid-connected pv power plants considering inverter limits," *International Journal of Electrical Power & Energy Systems*, vol. 149, p. 109045, 2023.
[34] "Recommended practice for calculating ac short-circuit currents in industrial and commercial power systems," *IEEE Std 551-2006 [The Violet Book]*, pp. 1–308, 2006.
[35] O. Gomis-Bellmunt *et al.*, "Steady-state impedance mapping in grids with power electronics: What is grid strength in modern power systems?," *International Journal of Electrical Power & Energy Systems*, vol. 136, p. 107635, 2022.
[36] J. Song, J. Fanals-Batllori, L. Marín, M. Cheah-Mane, E. Prieto-Araujo, E. Bullich-Massagué, and O. Gomis-Bellmunt, "A short-circuit calculation solver for power systems with power electronics converters," *International Journal of Electrical Power & Energy Systems*, vol. 157, p. 109839, 2024.